

Journal of Biomedical Optics

SPIEDigitalLibrary.org/jbo

Impact of one-layer assumption on diffuse reflectance spectroscopy of skin

Ricky Hennessy
Mia K. Markey
James W. Tunnell

Impact of one-layer assumption on diffuse reflectance spectroscopy of skin

Ricky Hennessy,^{a,*} Mia K. Markey,^{a,b} and James W. Tunnell^b

^aThe University of Texas, Biomedical Engineering, 107 West Dean Keeton Street, Austin, Texas 78712, United States

^bUniversity of Texas MD Anderson Cancer Center, Imaging Physics, 1515 Holcombe Boulevard, Houston, Texas 77030, United States

Abstract. Diffuse reflectance spectroscopy (DRS) can be used to noninvasively measure skin properties. To extract skin properties from DRS spectra, you need a model that relates the reflectance to the tissue properties. Most models are based on the assumption that skin is homogenous. In reality, skin is composed of multiple layers, and the homogeneity assumption can lead to errors. In this study, we analyze the errors caused by the homogeneity assumption. This is accomplished by creating realistic skin spectra using a computational model, then extracting properties from those spectra using a one-layer model. The extracted parameters are then compared to the parameters used to create the modeled spectra. We used a wavelength range of 400 to 750 nm and a source detector separation of 250 μm . Our results show that use of a one-layer skin model causes underestimation of hemoglobin concentration [Hb] and melanin concentration [mel]. Additionally, the magnitude of the error is dependent on epidermal thickness. The one-layer assumption also causes [Hb] and [mel] to be correlated. Oxygen saturation is overestimated when it is below 50% and underestimated when it is above 50%. We also found that the vessel radius factor used to account for pigment packaging is correlated with epidermal thickness. © The Authors. Published by SPIE under a Creative Commons Attribution 3.0 Unported License. Distribution or reproduction of this work in whole or in part requires full attribution of the original publication, including its DOI. [DOI: 10.1117/1.JBO.20.2.027001]

Keywords: diffuse reflectance spectroscopy; Monte Carlo; two-layer.

Paper 140644RR received Oct. 3, 2014; accepted for publication Jan. 12, 2015; published online Feb. 3, 2015.

1 Introduction

Diffuse reflectance spectroscopy (DRS) is an optical technique that has been widely used to noninvasively measure skin optical properties.¹⁻⁹ Typically, a DRS probe consists of a group of fibers that are placed in contact with the skin. The most common fiber orientation is the six-around-one geometry where a central fiber connected to a light source injects light into the tissue, and the six peripheral fibers collect the light that has travelled through the tissue and returned to the surface. This light contains quantitative information about the tissue that it has passed through, and this information can be used to assess the tissue's physiological state. A model that relates the diffuse reflectance to physiological properties of tissue is used to extract physiological parameters from the DRS spectra. Many models based on the diffusion approximation have been developed to extract properties from DRS spectra; however, this technique requires source detector separations (SDSs) of at least 1 mm.^{2,10,11} Because the thickness of the epidermis is on the order of 100 μm ,¹² SDSs much less than 1 mm are necessary in order to probe the epidermis properties, meaning the assumptions required for the diffusion approximation are invalid. To overcome this problem, recently developed models for extracting physiological properties from DRS spectra have used Monte Carlo (MC) simulations to model the transport of photons through tissue.¹³⁻¹⁵ Most of these models are based on the assumption that skin is homogeneous and that its properties are independent of depth. In reality, skin is composed of

multiple layers with different properties. For example, melanin is primarily located in the epidermis, whereas hemoglobin is only located in the dermis. Additionally, the thickness of the epidermis varies with anatomical location. Assuming that skin is homogenous can lead to errors in the extracted physiological properties because variations in epidermal thickness can make the measurement of chromophore concentrations difficult by changing the sensitivity of the probe to each layer. Some multilayered inverse models of skin have been developed to overcome this problem.¹⁶⁻²¹ While depth-dependent heterogeneities were analyzed in this study, heterogeneities that are spatially in the plane of detection were not considered. Such heterogeneities would include the border of a nevus or other concentrations of pigment in the skin as well as the localization of hemoglobin in vessels which was investigated by Fredriksson et al.²⁰ Additionally, Fredriksson et al. generated a spectra using a two-layer model of skin with individual blood vessels and fit those spectra with a one-layer model. They found that using the one-layer model led to much greater errors in extracted parameters when compared to using a three-layer model to fit the spectra.²⁰

In this study, we analyze the specific errors that are caused by the one-layer assumption of skin. This is accomplished by first creating modeled DRS spectra using a two-layered forward diffuse reflectance skin model in the 400 to 750 nm wavelength range with an SDS of 250 μm . Next, parameters are extracted from the spectra using an inverse one-layer, or homogenous, skin model. The extracted parameters can then be compared to the parameters used to generate the modeled two-layer spectra, and this allows for a quantitative and systematic analysis of the errors that arise from the homogeneity assumption for skin.

*Address all correspondence to: Ricky Hennessy, E-mail: hennessy@utexas.edu

2 Materials and Methods

2.1 Two-Layer Forward Model

Modeled spectra were created using a two-layer skin model based on an MC lookup table (MCLUT) approach.¹⁶ A four-dimensional MCLUT was created using a two-dimensional MC code written in ANSI C²² implemented on an NVIDIA GTX 560 Ti GPU on 386 parallel threads.²³ The refractive index above the tissue was set to 1.45 to match the refractive index of an optical fiber, and the refractive index of the medium was set to 1.4 to match the refractive index of tissue. Spatially resolved diffuse reflectance was calculated by convolving the impulse response using a Gaussian-shaped beam profile with a radius of 100 μm , and reflectance was calculated at a center-to-center SDS of 250 μm with a 100- μm radius collection fiber.²⁴ This geometry was chosen because of its common use in skin applications.²⁵ Each entry in the MCLUT contains a reflectance value for a given top layer thickness (Z_0), epidermal absorption ($\mu_{a,\text{epi}}$), dermal absorption ($\mu_{a,\text{derm}}$), and reduced scattering coefficient (μ'_s), which is assumed to be equal in both layers. In the MCLUT, Z_0 ranges from 0 to 1000 μm , $\mu_{a,\text{epi}}$ ranges from 0 to 50 cm^{-1} , $\mu_{a,\text{derm}}$ ranges from 0 to 50 cm^{-1} , and μ'_s ranges from 0 to 70 cm^{-1} . Ten evenly spaced increments were used for each of the parameters, giving a total of 10,000 separate MC simulations. A total of 10^7 photons were used for each MC simulation. The Henyey–Greenstein phase function was used for sampling scattering angles. Scattering anisotropy was set to 0.85 for all simulations.

The MCLUT-based forward model for diffuse reflectance is based on a two-layer skin model where a reference absorption spectrum of melanin²⁶ is used for the top layer and oxy- and deoxy- hemoglobin²⁷ spectra are used for the bottom layer with a wavelength range of 400 to 750 nm. Spectra are generated by first selecting the following properties: (1) epidermal thickness (Z_0), (2) hemoglobin concentration ([Hb]), (3) oxygen saturation (SO_2), (4) melanin concentration ([mel]), and (5) $\mu'_s(\lambda_0)$. Reduced scattering at all wavelengths is calculated using Eq. (1), which is commonly used in tissue optics,^{13–16}

$$\mu'_s(\lambda) = \mu'_s(\lambda_0) \times \left(\frac{\lambda}{\lambda_0}\right)^{-B}, \quad (1)$$

where μ'_s is the reduced scattering coefficient at wavelength λ , $\lambda_0 = 630$ nm, and B is the scattering exponent, which is related to the size of the scattering particles. Absorption in the top layer at each wavelength is calculated using Eq. (2)

$$\mu_{a,\text{epi}}(\lambda) = \varepsilon_{\text{mel}}(\lambda)[\text{mel}], \quad (2)$$

where $\mu_{a,\text{epi}}(\lambda)$ is the epidermal absorption coefficient at wavelength λ , $\varepsilon_{\text{mel}}(\lambda)$ is the extinction coefficient of melanin at wavelength λ , and [mel] is the concentration of melanin. Absorption in the bottom layer at each wavelength is calculated using Eq. (3),

$$\mu_{a,\text{derm}}(\lambda) = [\text{Hb}][\varepsilon_{\text{HbO}_2}(\lambda)\text{SO}_2 + \varepsilon_{\text{Hb}}(\lambda)(1 - \text{SO}_2)], \quad (3)$$

where $\mu_{a,\text{derm}}(\lambda)$ is the dermal absorption coefficient at wavelength λ , [Hb] is the total concentration of hemoglobin, $\varepsilon_{\text{HbO}_2}(\lambda)$ is the extinction coefficient of oxygenated hemoglobin at wavelength λ , $\varepsilon_{\text{Hb}}(\lambda)$ is the extinction coefficient of deoxygenated hemoglobin at wavelength λ , and SO_2 is the oxygen

saturation. Once the optical properties are determined at each wavelength, the MCLUT is used to determine the reflectance at each wavelength. Cubic splines are used to interpolate between values in the MCLUT.

2.2 One-Layer Inverse Model

A one-layer inverse skin model was used to extract the parameters from the two-layer spectra. The same code used to generate the two-layer MCLUT was also used to create the one-layer MCLUT. Refractive indices and probe geometry parameters were also the same. In the one-layer MCLUT, μ'_s ranges from 0 to 70 cm^{-1} and μ_a ranges from 0 to 50 cm^{-1} to cover the range of optical properties present in skin.²⁸ Ten evenly spaced increments were used for each parameter. In the one-layer inverse model, the first step is to set initial values to the following parameters: (1) $\mu'_s(\lambda_0)$, (2) [mel], (3) [Hb], (4) SO_2 , and (5) vessel radius (R_{vess}). Next, $\mu'_s(\lambda)$ is calculated using Eq. (1) and $\mu_a(\lambda)$ is determined using the following equation:

$$\mu_a(\lambda) = \varepsilon_{\text{mel}}(\lambda)[\text{mel}] + \mu_{a,\text{Hb}}^{\text{corrected}}(\lambda), \quad (4)$$

where [mel] represents the concentration of melanin and $\mu_{a,\text{Hb}}^{\text{corrected}}(\lambda)$ is the wavelength dependent absorption due to hemoglobin that has been corrected for the inhomogeneous distribution. Because hemoglobin is confined to very small volumes in blood vessels, we account for this inhomogeneous distribution in tissue by using the corrections described by van Veen et al. to calculate a corrected absorption coefficient of blood.²⁹ The correction factor can be calculated as

$$C_{\text{pack}}(\lambda) = \left[\frac{1 - \exp(-2\mu_{a,\text{bl}}(\lambda)r_{\text{vess}})}{2\mu_{a,\text{bl}}(\lambda)r_{\text{vess}}} \right], \quad (5)$$

where $\mu_{a,\text{bl}}(\lambda)$ is the absorption coefficient of whole blood and r_{vess} is assumed to be the mean vessel radius in the tissue volume sampled. The packaging corrected absorption coefficient of blood in tissue can now be written as

$$\mu_{a,\text{Hb}}^{\text{corrected}}(\lambda) = C_{\text{pack}}(\lambda)\mu_{a,\text{bl}}(\lambda), \quad (6)$$

where

$$\mu_{a,\text{bl}}(\lambda) = [\text{Hb}][\varepsilon_{\text{HbO}_2}(\lambda)\text{SO}_2 + \varepsilon_{\text{Hb}}(\lambda)(1 - \text{SO}_2)], \quad (7)$$

where [Hb] is the hemoglobin concentration, $\varepsilon_{\text{HbO}_2}(\lambda)$ is the extinction coefficient for oxygenated hemoglobin at wavelength λ , $\varepsilon_{\text{Hb}}(\lambda)$ is the extinction coefficient for deoxygenated hemoglobin at wavelength λ , and SO_2 is the oxygen saturation. After Eqs. (1), (4) to (7) are used to calculate $\mu_a(\lambda)$ and $\mu'_s(\lambda)$, the one-layer MCLUT is used to generate a reflectance spectrum. The root-mean-squared error between this spectrum and the modeled two-layer spectrum is then calculated. The parameters are then iteratively updated until the error is minimized. An interior-point nonlinear optimization routine provided in the MATLAB® optimization toolbox (Mathworks, Natick, Massachusetts) was used as the optimization algorithm. In order to avoid converging to a local minima, the optimization algorithm was run three times with three different sets of initialization parameters and then we used the solution that gave the smallest error. We are confident that the global minimum was

found because the three different initialization parameters led to very similar solutions.

2.3 Extracting One-Layer Properties from Two-Layer Spectra

By fixing some parameters and changing others in the two-layer forward model and then fitting the resulting two-layer spectra with the one-layer model, we are able to systematically determine the errors that arise from the homogeneity assumption of skin. The following experiments were performed:

1. changing [mel] and fixing all other two-layer parameters,
2. changing [Hb] and fixing all other two-layer parameters,
3. changing SO_2 and fixing all other two-layer parameters,
4. changing Z_0 and fixing all other two-layer parameters to analyze the relationship between Z_0 and r_{vess} , and
5. selecting random pairs of [mel] and [Hb] and fixing all other two-layer parameters.

3 Results

Spectra based on a two-layer skin model were generated and then parameters from the spectra were extracted using a one-layer inverse skin model. Figure 1 shows a representative fit and illustrates the good agreement between the two-layer and one-layer spectra. Because the same scattering value was used for both layers in the two-layer model, the error in extracted scattering values was always less than 1.7%. Figure 2 shows the two-layer [mel] versus the one-layer extracted [mel]. This plot was created by varying the two-layer [mel] used to create the spectra and fixing all other parameters at three different values for Z_0 (50, 100, and 200 μm). [Hb] was fixed at 1 mg/ml, μ'_s was fixed at 20 cm^{-1} , SO_2 was fixed at 100%, and B was fixed at -1.5 . [mel] ranged from 0 to 5

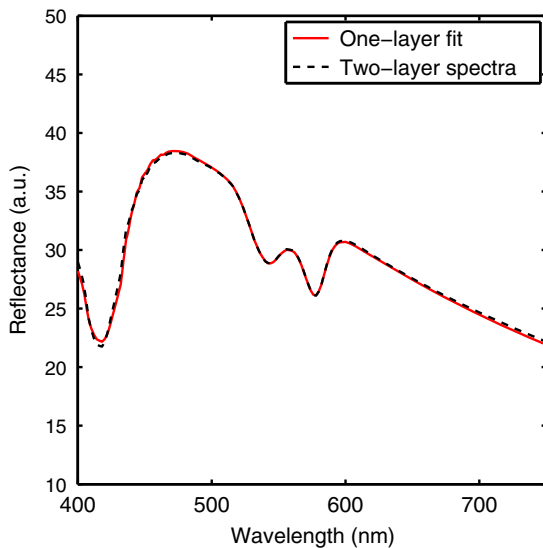


Fig. 1 A representative fit showing the good agreement between the two-layer and one-layer spectra.

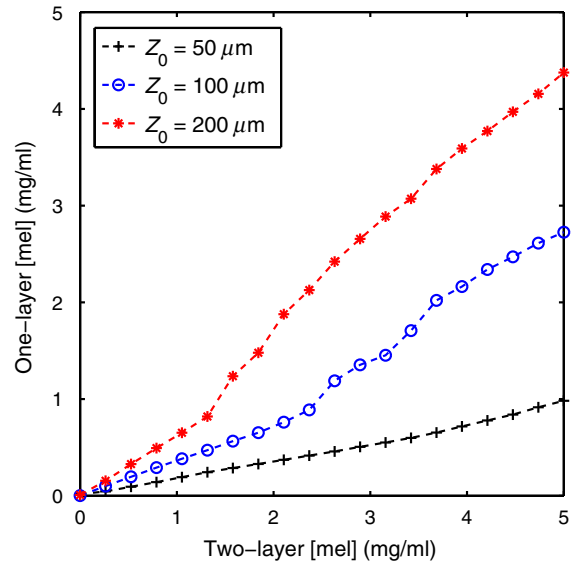


Fig. 2 Two-layer [mel] versus the one-layer extracted [mel]. This plot was created by varying the two-layer [mel] used to create the spectra and fixing all other parameters at three different values for Z_0 (50, 100, and 200 μm). [Hb] was fixed at 1 mg/ml, μ'_s was fixed at 20 cm^{-1} , SO_2 was fixed at 100%, and B was fixed at -1.5 . [mel] ranged from 0 to 5 mg/ml in 20 increments.

5 mg/ml in 20 increments. The one-layer inverse model was then used to extract [mel] from each spectra.

Figure 3 shows the two-layer [Hb] versus the one-layer extracted [Hb]. This plot was created by varying the two-layer [Hb] used to create the spectra and fixing all other parameters at three different values for Z_0 (50, 100, and 200 μm). [mel] was fixed at 1 mg/ml, μ'_s was fixed at 20 cm^{-1} , SO_2 was fixed at 100%, and B was fixed at -1.5 . [Hb] ranged from 0 to 3 mg/ml in 20 increments. The one-layer inverse model was then used to extract [Hb] from each spectra.

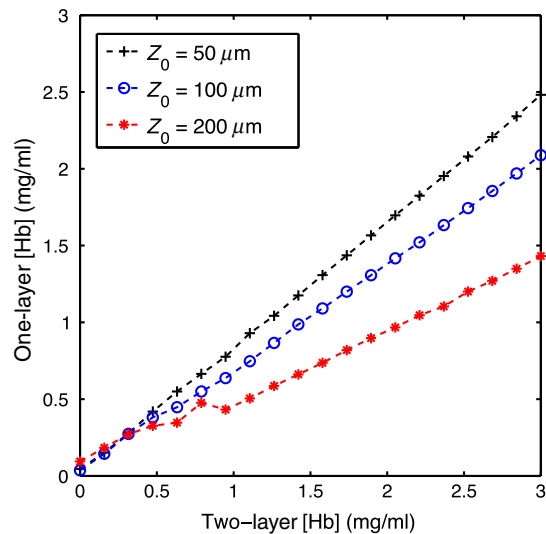


Fig. 3 Two-layer [Hb] versus the one-layer extracted [Hb]. This plot was created by varying the two-layer [Hb] used to create the spectra and fixing all other parameters at three different values for Z_0 (50, 100, and 200 μm). [mel] was fixed at 1 mg/ml, μ'_s was fixed at 20 cm^{-1} , SO_2 was fixed at 100%, and B was fixed at -1.5 . [mel] ranged from 0 to 3 mg/ml in 20 increments.

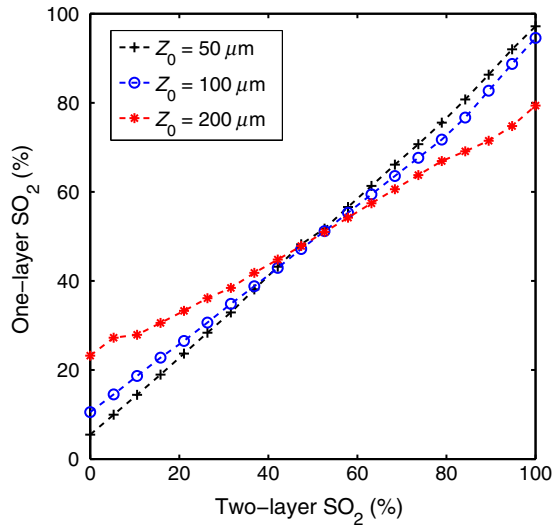


Fig. 4 Two-layer SO_2 versus the one-layer extracted SO_2 . This plot was created by varying the two-layer SO_2 used to create the spectra and fixing all other parameters at three different values for Z_0 (50, 100, and 200 μm). [mel] was fixed at 1 mg/ml, μ'_s was fixed at 20 cm^{-1} , [Hb] was fixed at 1 mg/ml, and B was fixed at -1.5 . SO_2 ranged from 0 to 100% in 20 increments.

Figure 4 shows the two-layer SO_2 versus the one-layer extracted SO_2 . This plot was created by varying the two-layer SO_2 used to create the spectra and fixing all other parameters at three different values for Z_0 (50, 100, and 200 μm). [mel] was fixed at 1 mg/ml, μ'_s was fixed at 20 cm^{-1} , [Hb] was fixed at 1 mg/ml, and B was fixed at -1.5 . SO_2 ranged from 0 to 100% in 20 increments. The one-layer inverse model was then used to extract SO_2 from each spectra.

Figure 5 shows Z_0 versus the vessel radius parameter used in the one-layer inverse model. This plot was created by varying Z_0 in the two-layer model used to create the spectra and fixing all other parameters. [mel] was fixed at 1 mg/ml, [Hb] was fixed at 1 mg/ml, μ'_s was fixed at 20 cm^{-1} , SO_2 was fixed at 100%, and B was fixed at -1.5 . Z_0 ranged from 0 to 300 μm in 20 increments.

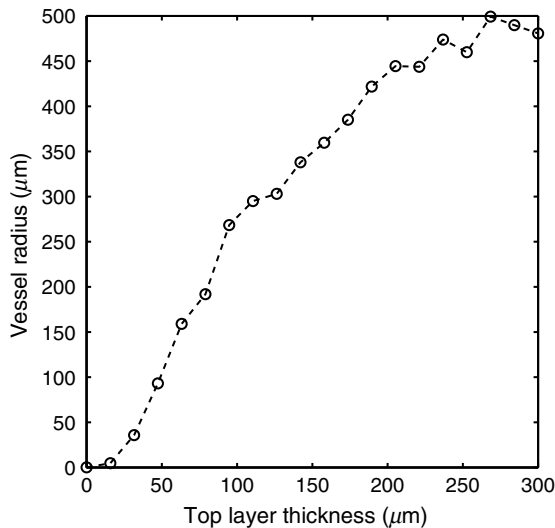


Fig. 5 Z_0 versus the vessel radius parameter used in the one-layer inverse model. This plot was created by varying Z_0 in the two-layer model used to create the spectra and fixing all other parameters. [mel] was fixed at 1 mg/ml, [Hb] was fixed at 1 mg/ml, μ'_s was fixed at 20 cm^{-1} , SO_2 was fixed at 100%, and B was fixed at -1.5 . Z_0 ranged from 0 to 300 μm in 20 increments.

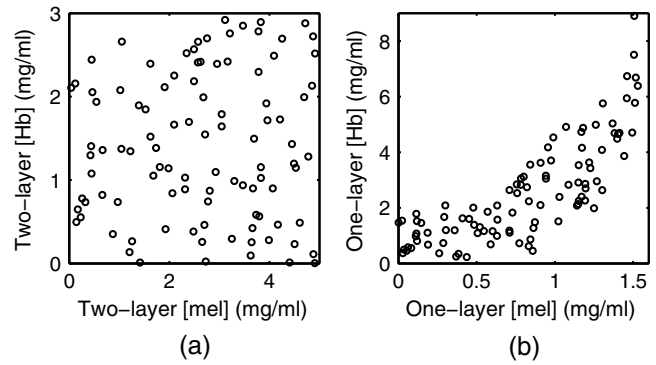


Fig. 6 (a) Random pairs of [Hb] and [mel] used to generate the two-layer spectra. (b) Extracted one-layer values for [Hb] and [mel].

1 mg/ml, μ'_s was fixed at 20 cm^{-1} , SO_2 was fixed at 100%, and B was fixed at -1.5 . Z_0 ranged from 0 to 300 μm in 20 increments. The one-layer inverse model was then used to extract vessel radius from each spectra. To illustrate the relationship between the pigment packaging factor in the one-layer model and the epidermal thickness, a pigment packaging factor was not included in the two-layer model.

Figures 6(a) and 6(b) were created by generating 100 random pairs of [mel] and [Hb] to generate two-layer spectra while all other parameters were fixed. Z_0 was fixed at 100 μm , μ'_s was fixed at 20 cm^{-1} , SO_2 was fixed at 100%, and B was fixed at -1.5 . The random pairs of [Hb] and [mel] used to generate the two-layer spectra are plotted in Fig. 6(a) and the extracted one-layer values for [Hb] and [mel] are plotted in Fig. 6(b). In Fig. 6(a), [Hb] and [mel] have a Pearson correlation coefficient (PCC) of $R = 0.0438$. In Fig. 6(b), [Hb] and [mel] have a PCC of $R = 0.7950$.

4 Discussion and Conclusions

In this study, we investigated errors caused by using a one-layer assumption for skin when using diffuse reflectance spectroscopy to measure optical properties. This was accomplished by first creating spectra using a two-layer skin model and then extracting the properties from the modeled spectra using a one-layer inverse skin model. The parameters used to generate the two-layer spectra were then compared to the parameters extracted with the one-layer inverse model.

Figure 2 shows the extracted one-layer [mel] versus the two-layer [mel] for three different epidermal thicknesses. Notice that the one-layer model underestimates [mel]; however, this would be expected since the one-layer inverse model is extracting a volume average for [mel], and the melanin is located only in a thin top layer. Additionally, the magnitude of the error is dependent on epidermal thickness, with an underestimation by a factor of 5 when the epidermal thickness is 50 μm and by a factor of approximately 1.25 when the epidermal thickness is 200 μm . If the epidermal thickness is unknown, it would not be possible to interpret a [mel] value extracted with a one-layer skin model. Similarly, Fig. 3 shows the extracted one-layer [Hb] versus the two-layer [Hb] for three different epidermal thicknesses. [Hb] is also underestimated when a one-layer skin model is used; however, the errors are smaller than the ones for [mel] and the relationship of the error to epidermal thickness is the opposite with an underestimation of a factor of 1.2 when the epidermal thickness is 50 μm and by a factor of 2 when the epidermal thickness is 200 μm . Figures 2 and 3 show that [Hb]

and [mel] will be underestimated when a one-layer skin model is used and that the magnitude of the underestimation is a function of epidermal thickness. If the epidermal thickness was known, it could be possible to correct for these errors; however, in many clinically realistic scenarios, the epidermal thickness will be unknown.

Figure 4 shows the extracted one-layer SO_2 versus the two-layer SO_2 for three different epidermal thicknesses. For $\text{SO}_2 < 50\%$, the one-layer model overestimates SO_2 , and for $\text{SO}_2 > 50\%$, the one-layer model underestimates SO_2 . The magnitude of the errors is directly proportional to epidermal thickness, meaning the error will be larger when the epidermis is thicker with error levels reaching 20% when the epidermal thickness is 200 μm . Similar to the problem with using a one-layer model to extract [mel] and [Hb], it will be difficult to interpret SO_2 values that are extracted using a one-layer skin model when the epidermal thickness is unknown.

To account for inhomogeneously distributed blood in skin, many one-layer models have incorporated a pigment packaging factor. This factor, often calculated as the average vessel radius, accounts for the flattening of the hemoglobin absorption spectra that is caused by the reduced path length of photons at wavelengths where the absorption is high. We noticed a similar flattening phenomenon is caused by increasing the epidermal thickness. Figure 5 was created in order to further investigate the relationship between the vessel radius factor in a one-layer model and the epidermal thickness in a two-layer model. Figure 5 shows that there is a strong positive correlation between epidermal thickness and the vessel radius factor. Because of this, we believe the pigment packaging factor is influenced by both the localization of blood in vessels and the localization of blood under the epidermis.

In Fig. 6, we investigate if the one-layer assumption would have any effect on the correlation between [mel] and [Hb]. First, random pairs of [mel] and [Hb] were selected and used to generate two-layer spectra. These random pairs are plotted in Fig. 6(a) and are essentially uncorrelated with a PCC of $R = 0.044$. Figure 6(b) plots the pairs of [mel] and [Hb] that were extracted using the one-layer model and shows that they are highly correlated with a PCC of $R = 0.795$. This correlation is due to the wavelength dependence of photon sampling depth. At shorter wavelengths, both scattering and absorption in skin are higher, therefore, photons with shorter wavelengths have shallower sampling depths and are more heavily weighted toward the properties of the epidermis.³⁰ This means that the effect of melanin is larger at shorter wavelengths in a two-layer model. In a one-layer model, this does not occur because hemoglobin and melanin are evenly distributed. When you attempt to fit a one-layer model to two-layer data, the one-layer model will underestimate the absorption due to melanin at shorter wavelengths. To compensate for this, the optimization routine can increase the hemoglobin concentration since hemoglobin absorbs strongly at shorter wavelengths. This allows the optimization routine to minimize the error, but causes the artificial correlation between melanin concentration and hemoglobin concentration. We believe that this is the biggest limitation of using a one-layer model since there is no way to correct for the artificial correlation between [mel] and [Hb]. Additionally, correlation between extracted parameters can decrease the performance of a classifier. For example, if the extracted parameters were used to train a classifier for the diagnosis of skin cancer, we would expect an inferior

performance from the classifier because of the artificial correlation between [mel] and [Hb] that is caused by the one-layer assumption of skin.

We have demonstrated evidence that using a one-layer model for skin to extract properties from DRS spectra leads to errors in the extracted properties. By generating modeled spectra with a more physiologically realistic two-layer model, and then extracting properties from those spectra using a one-layer inverse skin model, we were able to quantitatively and systematically analyze the errors that arise from the one-layer assumption for skin. All of our simulations were performed using a 400 to 750 nm wavelength range and an SDS of 250 μm since these values are common for DRS in skin. At longer wavelengths where the absorption due to hemoglobin and melanin is negligible, a one-layer model could be sufficient. Additionally, a one-layer model could also be sufficient for much larger SDSs where the effect of the epidermis is greatly diminished. The main disadvantage of using a two-layer model is the increased computational complexity; however, through the use of an LUT method and advances in GPU computing, this is no longer a major issue. Our results can be used to aid in the interpretation of extracted one-layer parameters; but more importantly, these results provide evidence showing that a one-layer model is inadequate for extracting optical properties from a two-layered tissue.

Acknowledgments

The funding for this project was provided by the NIH (R21EB015892), the NSF (DGE-1110007), and the Cancer Prevention and Research Institute of Texas (RP130702).

References

1. N. Rajaram et al., "Pilot clinical study for quantitative spectral diagnosis of non-melanoma skin cancer," *Laser Surg. Med.* **42**(10), 716–727 (2010).
2. G. Zonios, J. Bykowski, and N. Kollias, "Skin melanin, hemoglobin, and light scattering properties can be quantitatively assessed in vivo using diffuse reflectance spectroscopy," *J. Invest. Dermatol.* **117**, 1452–1457 (2001).
3. G. N. Stamatias et al., "In vivo measurement of skin erythema and pigmentation: new means of implementation of diffuse reflectance spectroscopy with a commercial instrument," *Brit. J. Dermatol.* **159**(3), 683–690 (2008).
4. L. Lim et al., "Probe pressure effects on human skin diffuse reflectance and fluorescence spectroscopy measurements," *J. Biomed. Opt.* **16**(1), 011012 (2011).
5. S. Tseng, A. Grant, and A. J. Durkin, "In vivo determination of skin near-infrared optical properties using diffuse optical spectroscopy," *J. Biomed. Opt.* **13**(1), 014016 (2008).
6. B. W. Murphy et al., "Toward the discrimination of early melanoma from common and dysplastic nevus using fiber optic diffuse reflectance spectroscopy," *J. Biomed. Opt.* **10**(6), 064020 (2005).
7. A. Garcia-Urbe et al., "In vivo characterization of optical properties of pigmented skin lesions including melanoma using oblique incidence diffuse reflectance spectroscopy," *J. Biomed. Opt.* **16**(2), 020501 (2011).
8. G. Zonios et al., "Melanin absorption spectroscopy: new method for noninvasive skin investigation and melanoma detection," *J. Biomed. Opt.* **13**(1), 014017 (2008).
9. E. Borisova et al., "Diagnostics of pigmented skin tumors based on laser-induced autofluorescence and diffuse reflectance spectroscopy," *Quantum Electron.* **38**(6), 597–605 (2008).
10. G. Zonios et al., "Diffuse reflectance spectroscopy of human adenomatous colon polyps in vivo," *Appl. Optics* **38**(31), 6628–6637 (1999).
11. R. M. P. Doornbos et al., "The determination of in vivo human tissue optical properties and absolute chromophore concentrations using spatially resolved steady-state diffuse reflectance spectroscopy," *Phys. Med. Biol.* **44**(4), 967–981 (1999).

12. T. Gambichler et al., "In vivo data of epidermal thickness evaluated by optical coherence tomography: effects of age, gender, skin type, and anatomic site," *J. Dermatol. Sci.* **44**(3) 145–152 (2006).
13. C. Zhu et al., "Diagnosis of breast cancer using diffuse reflectance spectroscopy: comparison of a Monte Carlo versus partial least squares analysis based feature extraction technique," *Laser Surg. Med.* **38**(7), 714–724 (2006).
14. G. M. Palmer and N. Ramanujam, "Monte Carlo-based inverse model for calculating tissue optical properties. Part I: theory and validation on synthetic phantoms," *Appl. Opt.* **45**(5), 1062–1071 (2006).
15. R. Hennessy et al., "Monte Carlo lookup table-based inverse model for extracting optical properties from tissue-simulating phantoms using diffuse reflectance spectroscopy," *J. Biomed. Opt.* **18**(3) 037003 (2013).
16. M. Sharma et al., "Verification of a two-layer inverse Monte Carlo absorption model using multiple source-detector separation diffuse reflectance spectroscopy," *Biomed. Opt. Express* **5**(1), 40–53 (2014).
17. Q. Liu and N. Ramanujam, "Sequential estimation of optical properties of a two-layered epithelial tissue model from depth-resolved ultraviolet-visible diffuse reflectance spectra," *Appl. Opt.* **45**(19), 4776–4790 (2006).
18. A. Kienle et al., "Noninvasive determination of the optical properties of two-layered turbid media," *Appl. Opt.* **37**(4), 779–791 (1998).
19. G. Mantis and G. Zonios, "Simple two-layer reflectance model for biological tissue applications," *Appl. Opt.* **48**(18), 3490–3496 (2009).
20. I. Fredriksson, M. Larsson, and T. Strömberg, "Inverse Monte Carlo method in a multilayered tissue model for diffuse reflectance spectroscopy," *J. Biomed. Opt.* **17**(4) 047004 (2012).
21. X. Zhong, X. Wen, and D. Zhu, "Lookup-table-based inverse model for human skin reflectance spectroscopy: two-layered Monte Carlo simulations and experiments," *Opt. Express* **22**(2), 1852–1864 (2014).
22. L. Wang, S. L. Jacques, and L. Zheng, "MCML – Monte Carlo modeling of light transport in multi-layered tissues," *Comput. Methods Programs Biomed.* **47**(2), 131–146 (1995).
23. E. Alerstam et al., "Next-generation acceleration and code optimization for light transport in turbid media using GPUs," *Biomed. Opt. Express* **1**(2), 658–675 (2010).
24. L. Wang, S. L. Jacques, and L. Zheng, "CONV—Convolution for responses to a finite diameter photon beam incident on multi-layered tissues," *Comput. Methods Programs Biomed.* **54**(3), 141–150 (1997).
25. U. Utzinger and R. R. Richards-Kortum, "Fiber optic probes for biomedical optical spectroscopy," *J. Biomed. Opt.* **8**(1), 121–147 (2003).
26. S. L. Jacques, R. D. Glickman, and J. A. Schwartz, "Internal absorption coefficient and threshold for pulsed laser distribution of melanosomes isolated from retinal pigment epithelium," *Proc. SPIE* **2681**, 468–477 (1996).
27. S. A. Prahl, "Optical absorption of hemoglobin," in *Tabulated Hemoglobin Spectra*, compiled by S. A. Prahl, Oregon Medical Laser Center, <http://omlc.org/spectra/hemoglobin/> (22 August 2014).
28. T. Lister, P. A. Wright, and P. H. Chappell, "Optical properties of human skin," *J. Biomed. Opt.* **17**(9) 090901 (2012).
29. R. L. van Veen, W. Verkuysse, and H. J. Sterenborg, "Diffuse-reflectance spectroscopy from 500 to 1060 nm by correction for inhomogeneously distributed absorbers," *Opt. Lett.* **27**(4), 246–248 (2002).
30. R. Hennessy et al., "Effect of probe geometry and optical properties on the sampling depth for diffuse reflectance spectroscopy," *J. Biomed. Opt.* **19**(10) 107002 (2014).

Ricky Hennessy is an NSF graduate research fellow in the Department of Biomedical Engineering at the University of Texas at Austin. He is advised by Drs. James W. Tunnell and Mia K. Markey. He earned his BS and MS degrees in biomedical engineering from California Polytechnic State University in San Luis Obispo. He will graduate with his PhD in February 2015.

Mia K. Markey is a full-time professor of biomedical engineering at the University of Texas at Austin and adjunct professor of imaging physics at the University of Texas at MD Anderson Cancer Center. A 1994 graduate of the Illinois Mathematics and Science Academy, she received her BS degree in computational biology (1998) from Carnegie Mellon University and a PhD degree in biomedical engineering (2002), along with a certificate in bioinformatics, from Duke University.

James W. Tunnell is an associate professor of biomedical engineering at the University of Texas at Austin. He earned his BS degree in electrical engineering from the University of Texas at Austin and his PhD degree in bioengineering from Rice University. He was awarded a National Research Service award from the NIH to fund his postdoctoral fellowship at MIT from 2003 to 2005. He joined the faculty of the University of Texas at Austin in the fall of 2005.